

# Large-Format Imaging Plate and Weissenberg Camera for Accurate Protein Crystallographic Data Collection Using Synchrotron Radiation

K. Sakabe,<sup>a†</sup> K. Sasaki,<sup>b†</sup> N. Watanabe,<sup>c†</sup> M. Suzuki,<sup>c†</sup> Z. G. Wang,<sup>c‡</sup>  
J. Miyahara<sup>d§</sup> and N. Sakabe<sup>e</sup>

<sup>a</sup>Department of Chemistry, Faculty of Science, Nagoya University, Nagoya 464, Japan,

<sup>b</sup>College of Medical Technology, Nagoya University, Higashi, Nagoya 461, Japan, <sup>c</sup>Photon Factory, National Laboratory for High Energy Physics, Tsukuba 305, Japan, <sup>d</sup>Fuji Photo Film Company Ltd, Kanagawa 258, Japan, and <sup>e</sup>Institute of Applied Biochemistry and Tsukuba Advanced Research Alliance (TARA), University of Tsukuba, Ibaraki 305, Japan. E-mail: sakabe@kekvox.kek.jp

(Received 23 January 1997; accepted 6 March 1997)

Off-line and on-line protein data-collection systems using an imaging plate as a detector are described and their components reported. The off-line scanner IPR4080 was developed for a large-format imaging plate 'BASIII' of dimensions 400 × 400 mm and 400 × 800 mm. The characteristics of this scanner are a dynamic range of 10<sup>5</sup> photons pixel<sup>-1</sup>, low background noise and high sensitivity. A means of reducing electronic noise and a method for finding the origin of the noise are discussed in detail. A dedicated screenless Weissenberg camera matching IPR4080 with synchrotron radiation was developed and installed on beamline BL6B at the Photon Factory. This camera can attach one or two sheets of 400 × 800 mm large-format imaging plate inside the film cassette by evacuation. The positional reproducibility of the imaging plate on the cassette is so good that the data can be processed by batch job. Data of 93% completeness up to 1.6 Å resolution were collected on a single axis rotation and the value of  $R_{\text{merge}}$  becomes 4% from a tetragonal lysozyme crystal using a set of two imaging-plate sheets. Comparing two types of imaging plates, the signal-to-noise ratio of the ST-VIP-type imaging plate is 25% better than that of the BASIII-type imaging plate for protein data collection using 1.0 and 0.7 Å X-rays. A new on-line protein data-collection system with imaging plates is specially designed to use synchrotron radiation X-rays at maximum efficiency.

**Keywords:** imaging plates; Weissenberg cameras; macromolecular crystallography; data-collection systems.

## 1. Introduction

Imaging plates possess very good characteristics as integration-type area detectors, namely a high detection quantum efficiency, a wide dynamic range, a linear response over a wide range, a high spatial resolution, a large active area size, a good uniformity of response, a high count-rate capability and a large active area. They have been widely used as detectors for protein crystallographic data collection using the camera method for the last ten years with synchrotron radiation. The first data-collection system using synchrotron radiation for protein crystallography was constructed with imaging plates and a screenless Weissenberg camera at the Photon Factory in 1987 (Sakabe, 1991). In this system a bio-imaging analyzer (BA) type of

imaging plate was used. However, this type of imaging plate was soon replaced by a BASIII, which has a much higher sensitivity. The regular sizes of the BA and BASIII plates which may be purchased from Fuji Film Company Ltd are 200 × 400 mm<sup>2</sup> and 201 × 252 mm<sup>2</sup>. The image reader for these two types of imaging plate, BA100, was developed by Fuji Film Company Ltd for scientific applications, and this reader has recently been replaced by a BAS2000, which is of compact size and low cost. The smaller size imaging plate, *i.e.* 200 × 400 mm<sup>2</sup>, is so convenient that it has been used for the last ten years with Weissenberg cameras at the Photon Factory for crystallographic data collection of macromolecules. However, in order to collect intensity data to a high resolution from macromolecular crystals with a large unit cell, the cassette radius of the camera needs to be large. With increasing sample-cassette distance, using constant-wavelength X-rays, the maximum resolution limit recorded on the imaging plate becomes lower. Therefore, in order to record higher resolution data, the development of a large active-area imaging plate is

† Guest researcher for the TARA Sakabe project.

‡ Present address: Beijing Synchrotron Radiation Facility, Institute of High Energy Physics, Chinese Academy of Sciences, Bin 2-7, PO Box 918, Beijing 100039, People's Republic of China.

§ Present address: Fuji Photo Film Company Ltd, Nishiazabu, Minato, Tokyo 106, Japan.

essential. Initially, the large active area,  $800 \times 400 \text{ mm}^2$ , of the imaging plate was produced by sticking four  $400 \times 200 \text{ mm}^2$  imaging-plate sheets to each other. After recording the diffraction intensities, each imaging-plate sheet was separated, and the intensity was measured using a Fuji BAS2000 imaging-plate reader. Such a technique, however, has two weaknesses: it is difficult to determine an accurate orientation matrix for data processing, and four imaging-plate sheets must be read and processed for each shot.

To overcome these weaknesses a large-format BASIII with plate dimensions  $400 \times 800 \text{ mm}^2$  was produced by Fuji Film Company Ltd. This size was determined by consideration of the following two factors: (i) the present manufacturing width of the imaging plate is limited by Fuji Film Company Ltd to 400 mm, (ii) the length of the large-format imaging plate was set at 800 mm on the grounds of ease of operation in a dark hutch. We have developed an image reader (IPR4080) for this new large-format imaging plate.

The first camera which well matched this new large-format imaging plate was a time-resolved Laue camera which can also be used as a screenless Weissenberg camera with monochromatic X-rays (Sakabe *et al.*, 1995). The first dedicated Weissenberg camera with this new large-format imaging plate was designed for the TARA Sakabe research project. The data-collection systems with this Weissenberg camera and off-line imaging-plate reader, IPR4080, were constructed on BL6B at the Photon Factory. Automatic data-collection systems with on-line imaging-plate readers have been developed by many companies for laboratory X-ray sources and a few of them have been used with synchrotron radiation X-rays. However, their imaging-plate reading speed is very slow compared with the short exposure time achieved with a strong synchrotron radiation X-ray source. Thus, we began to design an automatic protein data-collection system with an imaging-plate reading speed well matched to the synchrotron radiation source.

Here we describe (a) a large-format image reader, IPR4080, (b) a protein data-collection system with a dedicated Weissenberg camera and  $400 \times 800 \text{ mm}^2$  large-format imaging plate, (c) the evaluation of a standard type V for Fuji computed radiography (ST-V) type of imaging plate in comparison with the BASIII which is normally used in the camera method for protein data collection, and (d) the design of a new automatic data-collection system well matched to synchrotron radiation X-ray intensities at the Photon Factory bending-magnet beamline.

## 2. Large-format imaging-plate reader IPR4080

The large-format imaging-plate reader, IPR4080, is an off-line scanner for two sizes of imaging plate, namely  $800 \times 400 \text{ mm}^2$  and  $400 \times 400 \text{ mm}^2$ . The imaging plate is automatically rolled up on the drum of the scanner and the stored images are read out by measuring the intensities of the luminescence, which is stimulated by a 35 mW HeNe

**Table 1**  
Format of IPR4080.

Type	Drum type: set imaging plate by reducing pressure
Rotation speed	500 r.p.m. (reading time 8 min)
Type of imaging plate	Fuji BASIII
Imaging-plate size	$400 \times 400 \text{ mm}^2$ , $400 \times 800 \text{ mm}^2$
Detector	Photomultiplier, type 1847-07 (Hamamatsu photonics)
Light source	HeNe gas laser ( $\lambda = 633 \text{ nm}$ , 35 mW)
Spot size	$30 \mu\text{m}$
ADC	Linear, $2^{16}$ (65 536 level)
Grey level	$65\,536 \times 4 = 262\,144$
Dynamic range	$10^5$ order
Sensitivity	1–2 X-ray photons
Host computer	IRIS-INDY
Total time	10 min (from putting in to removal of imaging plate)
Pixel size	$100 \times 100 \mu\text{m}$

$30 \mu\text{m}$  laser-focused spot on the phosphor surface. The pixel size of the readout is  $100 \times 100 \mu\text{m}^2$ . To reduce the electronic noise, four times sampling by an analog-to-digital converter (ADC) is performed in reading  $100 \mu\text{m}$  and the digital values are summed up. In such a way the grey level becomes four times larger than that of the ADC. The dynamic range of this imaging-plate reader achieved  $1\text{--}10^5$  X-ray photons per pixel using one photomultiplier when the high-voltage supply for the photomultiplier was set to 500 V. The format of the IPR4080 is summarized in Table 1.

In order to construct the imaging-plate reader with high sensitivity, special attention has been paid to reducing the electronic noise. The source of the electronic noise can be classified into the following three categories: (i) the low-voltage power supply, (ii) the high-voltage power supply for the photomultiplier, and (iii) the electromagnetic induction.

(i) *Noise from the low-voltage power supply for the photomultiplier.* It is easy to reduce the ripple with large capacitance. Very often this kind of noise comes from the ground and from the power supply, especially in a synchrotron radiation facility because the synchrotron radiation ring produces a very large amount of noise. A noise-reducing transformer is essential. Computers and pulse motor drivers are also origins of noise.

(ii) *Noise from the high-voltage supply for the photomultiplier.* Even though this kind of noise is small it is very harmful because the variation of the high-voltage supply for the photomultiplier affects the gain of the tube. This means that, unlike the former noise, this noise is enlarged in proportion to the input photons of the photomultiplier. After an imaging plate is exposed homogeneously in the stepwise increment of the X-ray dose, we read out the images. If the noise image is observed only in the low-dose region then the noise will not be caused by the high-voltage supply. However, if the noise images appear in the high-dose region in proportion to the X-ray dose, it must be caused by the high-voltage supply. The filters consisting of a  $100 \text{ k}\Omega$  resistor and a  $1 \mu\text{F}$  oil condenser were found to be effective.

(iii) *Noise caused by electromagnetic induction.* This type of noise is the most difficult to eliminate. The following techniques are rather classical; however, they are still effective. (a) Shield out sources of origins of noise which can effectively be detected by an oscilloscope with a small antenna. Since an electric circuit, especially the computer board in the reader, wire leads for the power supply, laser unit and pulse motor are also strong sources of noise, they must be shielded. (b) To protect the signal line from the induction noise, a linear amplifier must be placed in close proximity to the photomultiplier socket and should be well shielded. A coaxial cable was used as usual to lead the signal to the ADC unit. (c) All lead-in wires must be as short as possible. (d) A filter containing a variable resistor was placed before the ADC input in order to reduce the electronic noise and to maintain good frequency characteristics, as shown in Fig. 1. In most cases the sizes of the diffraction spots are larger than 0.4 mm in half width. If the shape of these diffraction spots along the laser scanning direction approximates to a sine curve, frequency characteristics of the electronic circuit must be flat in the range 0–7 kHz. An oscillator was connected to the input of the amplifier and the frequency characteristics were determined by measuring the voltage between the ADC input and the ADC ground with an oscilloscope. When  $R$  in Fig. 1 was set to 250  $\Omega$ , no decay was observed at 10 kHz and  $\sim 4\%$  decay was observed at 20 kHz.

The linearity of the response between the X-ray dose and the digital output of IPR4080 was measured using the same method as that reported by Miyahara, Takahashi, Amemiya, Kamiya & Satow (1986) using monochromatized Cu  $K\alpha$  X-rays from a sealed-tube X-ray generator. The result is shown in Fig. 2 where the digital outputs of the imaging-plate reader against X-ray photons per pixel are plotted. The maximum value of digital output is 262 144 ( $4 \times 2^{16}$ ). Fig. 2 shows the observed values when the high-tension supply voltage for the photomultiplier is set to 500 and 700 V. In the region lower than 100 photons pixel<sup>-1</sup> the observed values gradually deviate from a straight line and converge to  $\sim 20$  when a bias is set in order to protect the digital output being zero due to the electronic noise of the reader. The bias was set to about five times the noise value, which was the value read from the erased imaging plate. The corrected digital output value after subtracting the bias is shown in Fig. 2. An excellent linearity is observed

between the X-ray dose and the digital output in all regions, illustrating that the reader can be used up to  $10^5$  X-ray photons pixel<sup>-1</sup> at 500 V.

The high sensitivity and wide-range linear response of this imaging-plate reader as a part of the protein data-collection system has already been evaluated on BL18B equipped with a Weissenberg camera and BASIII-type imaging plate in comparison with Fuji BAS2000 and BA100 imaging-plate readers (Sakabe *et al.*, 1995). The sensitivity of IPR4080 is comparable with that of BA100 and hence better than that of BAS2000 by a factor of two, and the dynamic range of the reader, *i.e.* linear response to the X-ray dose, at a high-tension voltage of 500 V is ten times larger than those of BA100 and BAS2000.

### 3. Weissenberg camera with large-format imaging plate

A time-resolved Laue camera with large-format imaging plate is installed at bending-magnet beamline BL18B. This camera can also be operated with monochromatic X-rays in a Weissenberg mode. The outline and performance as a Weissenberg camera has been described previously (Sakabe *et al.*, 1995). This camera has two types of cassette which are fixed to the camera permanently and whose radii are 430 or 1290 mm. One and two large-format imaging plates can be fixed to the inside of the 430 and 1290 mm cassettes, respectively, by evacuation from the back of the cassette. This helps to maintain the radius of the imaging plate accurately over the whole area of the cassette. Since this camera has enough space around the sample, additional instruments can be attached easily. This camera is highly suitable for cryocrystallography and for tracing reactions using the large-oscillation technique (Kamiya, Sasaki, Watanabe, Sakabe & Sakabe, 1997). To reduce the background noise resulting from the scattering of the direct X-ray beam by air, a small helium path can be set between the sample and the main helium path where the beam stop is installed when we do not use an attachment.

The first dedicated Weissenberg camera with two large-format imaging-plate sheets ( $400 \times 800$  mm<sup>2</sup>) has been developed and installed at BL6B on bending-magnet beamline No. 6 at the Photon Factory. The overall optical

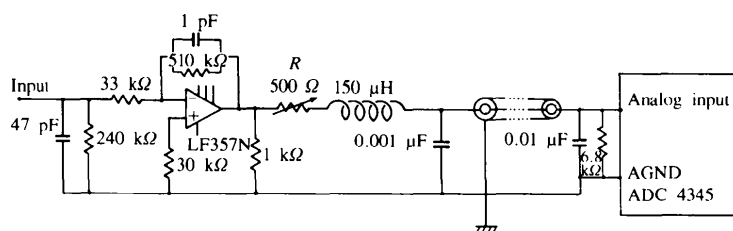


**Figure 1**

Part of the electric circuit of IPR4080. The best compromise between frequency characteristics and low electric noise was selected using a variable resistor.

configuration is very similar to that of BL6A (Sakabe, 1991). The brightness of the beam using 1.0 Å X-rays is about two or six times stronger than those of BL6A or BL18B, respectively. Photographs of this camera in the hutch are shown in Fig. 3. Although the cassette is very heavy, movement of the cassette is smooth because the rotation shaft of the imaging-plate cassette is on the centre of gravity of the cassette. Although the cylindrical cassette radius is 575.7 mm, the distance between the sample crystal and the cassette can be changed to between 575.7 and 968.0 mm. The resolution limits of the data along the vertical and horizontal directions are 1.5 and 1.8 Å, respectively, at a camera distance of 575.7 mm using 1.0 Å X-rays, and are 2.5 and 2.6 Å, respectively, at the maximum camera distance of 968 mm. The data-collection system consists of the Weissenberg camera and two IPR4080 imaging-plate readers to read two imaging-plate sheets which are set either horizontally or vertically by the support of mechanical guides.

### 3.1. Evaluation of the data-collection system

The evaluation of the data-collection system was carried out using hen egg white lysozyme crystals, whose crystal system is tetragonal, with space group  $P4_32_12$  and cell dimensions  $a = b = 79.6$ ,  $c = 38.2$  Å.

3.1.1. *Intensity-data measurement.* Large-format imaging plates were set in three different configurations to examine all possible setting cases.

(a) One sheet of the imaging plate is set in the middle of the cassette so that the 800 mm side is set along the arc of the film cassette. This setting is called case A, and the active detector area is  $800 \times 400$  mm<sup>2</sup>.

(b) The 800 mm sides of two imaging-plate sheets are set along the arc of the film cassette. This setting is called case B, and the active detector area is  $800 \times 800$  mm<sup>2</sup>.

(c) The 400 mm sides of two imaging-plate sheets are set along the arc of the cassette. This setting is called case C, and the active detector area is  $800 \times 800$  mm<sup>2</sup>.

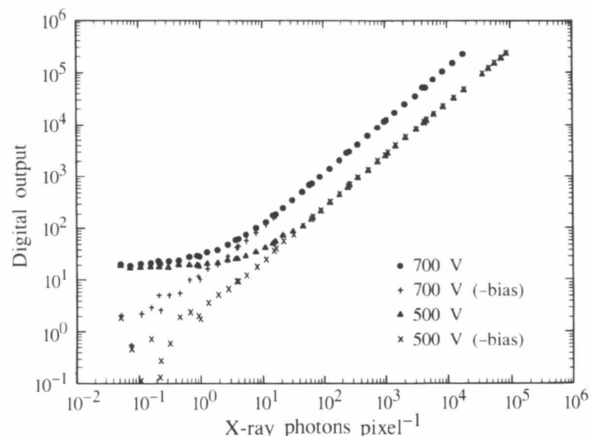
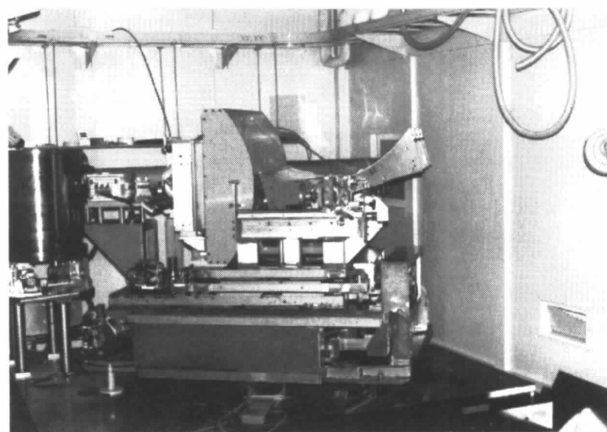


**Figure 2**  
Linear response curve between the X-ray dose and the digital output of the imaging-plate reader IPR4080.

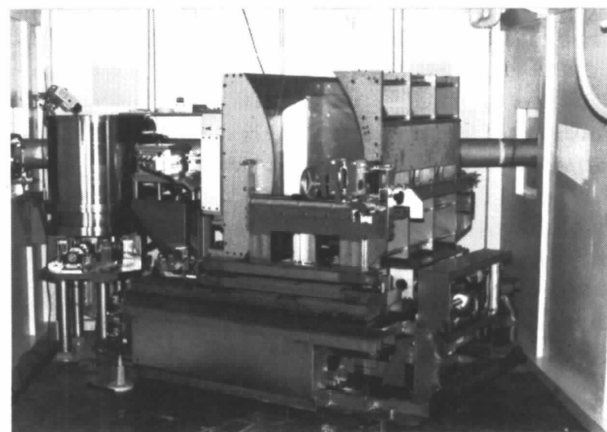
**Table 2**  
Data-collection conditions.

X-ray wavelength	1.0 Å
Cylindrical cassette radius	575.7 mm
Effective imaging-plate area:	
Case A	400 (H) × 800 (V) mm with one imaging-plate sheet
Cases B and C	800 (H) × 800 (V) mm with two imaging-plate sheets
Oscillation range	20° frame <sup>-1</sup>
Coupling constant	4° mm <sup>-1</sup>
Exposure time	200 s
Imaging-plate reader	IPR4080
Total frame number	5
Diameter of collimator	0.2 × 0.2 mm <sup>2</sup>
Crystal	Tetragonal lysozyme
Orientation of crystal	X-rays along <i>c</i> axis

Data collection was carried out under the conditions shown in Table 2. Two oscillation photographs were taken at 0 and 45° to determine the orientation matrix before and after the measurement of intensity data by the Weissenberg mode. The intensity data from the large-format imaging plate were processed with the *Denzo* program (Otwinowski



(a)



(b)

**Figure 3**  
Photographs of the dedicated Weissenberg camera for large-format imaging plates on BL6B at the Photon Factory. (a) Film cassette open, (b) film cassette closed.

**Table 3**

Difference in the direct-beam position on each imaging-plate sheet.

A, B: film rotation 180°. C: film rotation 90°. Units: mm.

Case	A		B				C			
	Middle		Left side		Right side		Upper side		Lower side	
	x	y	x	y	x	y	x	y	x	y
1	201.872	396.881	2.321	396.931	-401.174	392.750	397.927	-401.846	-0.472	396.862
2	201.792	396.978	1.855	396.797	-400.844	393.045	397.993	-402.662	-0.268	396.964
3	202.287	393.337*	2.590	396.689	-401.236	392.941	397.841	-402.148	-0.208	397.013
4	201.933	397.158	2.200	396.889	-400.782	392.569	397.635	-402.777	-0.209	397.212
5	202.443	393.263*	2.044	396.944	-401.077	392.029	397.738	-403.228	-0.350	397.713
Average	201.87	397.01	2.202	396.85	-401.02	392.67	397.83	-402.53	-0.301	397.15
R.m.s.	0.07	0.14	0.278	0.107	0.200	0.400	0.143	0.543	0.111	0.338

\* Different imaging-plate reader.

**Table 4**Completeness and percentage of the data larger than  $3\sigma|F|$  in each shell.Comp: completeness of data. %: data larger than  $3\sigma|F|$ .

Case Resolution (Å)	A			B			C		
	N	% Comp	%	N	% Comp	%	N	% Comp	%
7.02	147	59.6	98.6	133	54.8	98.5	155	62.1	100.0
5.02	350	91.9	100.0	334	89.0	100.0	348	91.5	100.0
4.11	433	92.6	99.1	414	89.4	99.5	427	90.9	99.8
3.56	533	98.0	99.4	512	95.6	99.6	525	96.8	99.8
3.19	602	98.5	99.7	587	97.4	99.7	601	98.9	99.2
2.92	638	96.0	98.1	634	95.9	98.1	660	98.7	98.5
2.70	662	93.2	98.0	678	95.4	98.4	690	96.7	97.8
2.53	683	90.5	99.0	704	93.0	99.1	725	95.4	99.4
2.38	707	88.3	98.2	770	95.6	98.7	782	96.7	98.0
2.26	746	88.8	97.2	810	95.6	98.3	819	96.6	97.4
2.16	783	89.1	96.4	835	94.5	96.6	853	96.0	96.1
2.06	809	88.6	96.8	870	94.5	96.9	897	96.7	97.7
1.98	823	86.7	94.9	893	93.5	96.1	922	95.8	94.9
1.91	818	83.2	92.9	921	93.4	96.1	938	94.0	94.6
1.85	836	81.9	92.2	950	93.1	93.7	1002	97.4	94.0
1.79	828	78.9	90.0	996	94.5	93.0	1005	94.8	91.3
1.74	837	77.1	85.2	1024	94.4	89.4	1013	92.8	87.6
1.69	827	74.1	82.6	1055	94.5	86.4	1038	92.6	86.9
1.64	800	70.0	80.6	1056	92.3	84.0	1036	90.2	81.0
1.60	792	67.2	76.0	1072	91.2	78.0	1064	90.3	77.2
Total	13 654	83.4	92.7	15 248	93.4	93.6	15 500	94.3	93.1

& Minor, 1996). In order to correct the rotation of the imaging plate from the direction of the spindle axis when the imaging plate is attached to the cassette, we made 3–5 fiducial points parallel to the direction of the spindle axis by the attenuated direct beam in these experiments.

(a) Case A. In order to process the data with *Denzo* as a batch job, it is essential that the direct-beam position is not much different among the imaging-plate sheets. Table 3 shows that the direct-beam positions are fixed quite well, except two values (marked by \*) which are read out by a different imaging-plate reader. The standard deviation of the beam position from the same reader is one pixel. The beam position on the imaging plate read out by the different imaging-plate reader, however, is different by 40 pixels and it is necessary to input the beam position before processing.

(b) Case B. Fiducial points on each imaging-plate sheet were marked by the attenuated direct beam, namely mark positions (30, 20, 5), (0, -5, -10, -15, -20) mm near the middle of the horizontal direction of the imaging plates,

where 0 is the direct-beam position in reflection data recording. Five sheets of the imaging plate set on the left side of the cassette were measured with IPR4080 and the other five imaging-plate sheets set on the right side of the cassette were measured by the other imaging-plate reader. The standard deviation of the error of beam positions is 5 pixels, and it is possible to process the data by batch job.

(c) Case C. In order to mark fiducial points on both sheets in case C, the cassette was moved by 10 mm up from the standard level to mark the lower side of the imaging plate and again 10 mm down to mark the upper side of the imaging plate. In total, eight fiducial marks were made at 0, 5, 20 and 30 mm on both sides. The standard deviation of the errors is 5 pixels. The maximum deviation is 7 pixels; however, it is still in the convergence region by the refinement of the orientation matrix.

Comparison of the data was performed using the *mtz* file of the *CCP4* suite of programs for protein crystallography (Collaborative Computing Project, Number 4, 1994).

**Table 5**

Comparison of the data collected by FAST and data collected by Weissenberg camera at different imaging-plate settings on the film cassette in each shell; cases A, B, C.

$N$  = number of data.  $R = \Sigma|F_1| - |F_2|/\Sigma|F_1|$ .

Case between $F_1$ and $F_2$ Resolution (Å)	FAST and A		FAST and B		FAST and C		A and B		A and C		B and C	
	$N$	$R$	$N$	$R$	$N$	$R$	$N$	$R$	$N$	$R$	$N$	$R$
7.07	30	0.046	30	0.046	33	0.040	29	0.021	32	0.027	32	0.022
5.00	258	0.036	239	0.041	258	0.040	243	0.020	261	0.025	242	0.017
4.08	389	0.038	379	0.042	386	0.043	392	0.017	401	0.022	392	0.012
3.54	483	0.043	455	0.041	472	0.044	456	0.014	475	0.019	451	0.010
3.16	592	0.044	580	0.043	590	0.043	583	0.012	596	0.018	582	0.010
2.89	650	0.048	636	0.046	665	0.047	631	0.011	650	0.016	636	0.009
2.67	661	0.049	669	0.050	688	0.049	650	0.012	660	0.016	668	0.011
2.50	692	0.050	712	0.048	733	0.049	677	0.011	693	0.015	712	0.010
2.36	727	0.054	777	0.053	801	0.054	712	0.014	727	0.018	775	0.013
2.24	753	0.054	810	0.054	828	0.055	736	0.016	754	0.020	809	0.017
2.13	780	0.063	844	0.064	863	0.066	770	0.020	785	0.026	846	0.022
2.04	803	0.060	852	0.061	884	0.065	799	0.023	818	0.031	871	0.026
1.96	754	0.071	831	0.072	857	0.081	814	0.027	833	0.041	908	0.038
1.89	760	0.082	849	0.083	881	0.095	833	0.037	854	0.055	937	0.049
1.83	721	0.089	841	0.090	883	0.111	825	0.043	851	0.068	969	0.061
1.77	732	0.112	881	0.122	901	0.154	831	0.063	841	0.097	998	0.091
1.71	730	0.124	891	0.136	890	0.166	832	0.074	827	0.114	1018	0.107
1.67	732	0.156	897	0.182	892	0.211	820	0.107	806	0.129	1030	0.119
1.62	704	0.152	877	0.177	856	0.202	797	0.107	781	0.135	1038	0.130
1.58	728	0.178	911	0.202	861	0.225	795	0.128	765	0.155	1026	0.154
Total	12 679	0.062	13 961	0.0671	4222	0.071	13 225	0.026	13 410	0.035	14 940	0.031

**3.1.2. Evaluation of the data.** Table 4 shows the number and completeness of the data in each shell between 20 and 1.6 Å and the percentage of the data whose intensities are larger than  $3\sigma(F)$ . The total number of individual reflections thus obtained is 13 654, 15 248 and 15 500 in cases A, B and C, respectively. Although there is completeness of the overall data from a single imaging-plate sheet, case A is 83.4% and that of the two imaging-plate sheets in cases B and C are 93.6 and 94.3%, respectively. These results show that the use of two imaging-plate sheets is effective for increasing the number of independent reflections and the effectiveness is prominent in a high-resolution region. The quality of data is very good because the ratio of the data larger than  $3\sigma(F)$  is  $\sim 93\%$ . The completeness of the data in the outer shell at 1.6 Å is 91.2 and 90.3% in cases B and C, respectively, and the data greater than  $3\sigma$  is 78.0 and 77.2% at 1.6 Å resolution in cases B and C, respectively.  $R_{\text{merge}}(I)$  values between 20 and 1.6 Å resolution for cases A, B and C are 4.3, 4.0 and 4.5%, respectively. Table 5 shows a comparison between the data whose internal  $R_{\text{merge}}$  value is 3.4% in the resolution range 27.3–1.48 Å, given by Harada (1996), which were collected using a FAST detector manufactured by Nonius Co. Ltd, and the data in each case A, B and C and that among data sets A, B and C. The overall  $R$  values between the FAST data and each data set A, B and C are 6.2, 6.7 and 7.1%, respectively, whereas the overall  $R$  values among the cases A, B and C are between 2.6 and 3.5%. The  $R$  value between cases B and C in the commonly used resolution range for refinement lower than 2.13 Å is less than 2.2%. These results demonstrate that highly accurate data of high completeness can be collected using this data-collection system.

#### 4. Comparison between BASIII and ST-V imaging plates using IPR4080

Since protein crystals are easily damaged by X-rays it is important to create a detector with a high sensitivity and a high signal-to-noise ratio. Many kinds of ST-type imaging plates have been developed by Fuji Film Company Ltd for medical diagnostic purposes whereas BAS-type imaging plates have been developed for scientific research using techniques such as autoradiography, electron microscopy and X-ray crystallography. Originally we used the BA-type imaging plate and then the BASIII, whose sensitivity is about 20% higher than that of the BA imaging plate. We have collected data with BASIII using X-rays of wavelength mainly between 1 and 2 Å at the Photon Factory for the last ten years. However, X-rays of wavelength shorter than 1 Å are often required in order to reduce the radiation damage of the protein crystals and for the effective use of the anomalous-dispersion effect of metals such as Xe, whose adsorption edge is 0.3 Å, and which can be accommodated at the cavity of the protein with moderate gas pressure at a range between 1 and 100 atm. However, the ratio of X-rays passing through the imaging plate increases at shorter wavelengths and the sensitivity of the imaging plate becomes low. Then a thicker layer of photostimulable phosphor of barium fluorobromide containing a trace amount of bivalent europium as a luminescence centre, formulated as BaFBr:Eu<sup>2+</sup>, of the imaging plate may be suitable for hard X-rays. However, thicker layers of the photostimulable phosphor are likely to lose the sharpness of the image, *i.e.* the spatial resolution will become worse. ST-V-type imaging plates have a 1.6 times

**Table 6**

Data-collection conditions for comparison between ST-V-type and BASIII-type imaging plates.

Imaging plate	ST-V, BASIII
X-ray wavelength	0.7 or 1.0 Å
Cylindrical cassette radius	430 mm
Effective imaging-plate area	400 (H) × 400 (V) mm × 2
Oscillation range	10° frame <sup>-1</sup>
Coupling constant	2° mm <sup>-1</sup>
Exposure time	120 min (0.7 Å), 120 s (1.0 Å)
Beamline	BL18B
Collimator size	0.2 × 0.2 mm <sup>2</sup>
Imaging-plate reader	IPR4080
Crystal	ω-amino acid pyruvate aminotransferase

thicker photostimulable phosphor layer than the BASIII-type. Thus, the characteristics of BASIII-type and ST-V-type imaging plates were compared using 0.7 and 1.0 Å synchrotron radiation X-rays.

The experiment was carried out at BL18B with the camera in Weissenberg mode using a 430 mm film cassette. One sheet of BASIII and one sheet of ST-V of dimensions 400 × 400 mm<sup>2</sup> were set on the cassette at the same time and exposed to X-rays in order to remove the effect of variation of the beam during a rather long exposure time of 120 min. The sensitivity and signal-to-noise ratio was measured by changing the voltage to the photomultiplier in steps of 100 V in the range 400–800 V. Since the shape of the spots is different at the upper and lower sides along the arc of the cassette, the measurements were repeated twice; the first time with the ST-V plate in the upper position and the second time with the BASIII plate in the upper position. Finally, in order to check the reproducibility of the experiment, the measurements were made at the same setting condition as the first time. Each 400 × 400 mm imaging plate was read by IPR4080. The orientation of the crystal was not changed during the experiments. In order to obtain an accurate orientation matrix we calculated it from the oscillation image on one sheet of BASIII-type 400 × 800 mm<sup>2</sup> imaging plate recorded at the same setting as at the beginning of the experiment, and it was also confirmed from the oscillation image taken at the start and the end of the experiment that the orientation matrix had not changed. Two images on two types of imaging plates recorded at the upper and lower sides were merged to reduce the systematic errors caused by the different locations on the cassette. The experimental conditions are summarized in Table 6. Data processing was carried out using the program *WEIS* (Higashi, 1989). The thickness of the photostimulable phosphor layer of the ST-V-type imaging plate is 230 μm and that of the BASIII-type is 140 μm. If the broadening of the half width of the diffraction image is in proportion to the thickness of the phosphor, the expected value of the ratio is 1.64. The ratio of the half width between the ST-V and BASIII types is 1.0–1.1 and no obvious difference is observed between the two wavelengths. Thus, the broadening of a diffraction spot is less than 10%, which is small in comparison with the

**Table 7**

Comparison between BASIII-type and ST-V-type imaging plates.

$\sigma = F^2/(r.m.s.)^2$ . The final column represents the wavelength of the X-rays used for data collection.

	BASIII	ST-V	ST-V/BASIII	Wavelength
Thickness	140 μm	230 μm	1.64	
Sensitivity			1.2–1.5	
Half width	0.38–0.46 mm	0.42–0.45 mm	1.0–1.1	1 Å
$\langle\sigma\rangle$	19	24	1.26	1 Å
Half width	0.38 mm	0.425 mm	1.12	0.7 Å
$\langle\sigma\rangle$	18.5	23.2	1.25	0.7 Å

expected value based simply on the increase in the thickness of the phosphor. Broadening of the diffraction spots caused by the difference in focused beamline optics and crystal mosaicity for the two wavelengths may be larger than that caused by the increase in thickness. Thus, at least for the Photon Factory beamlines, the increase in spot broadening due to increased thickness of the ST-V imaging plate is of no significant consequence for protein crystallographic data collected at 0.7 and 1.0 Å, respectively. The average value of  $F^2$  per  $\sigma F^2$  ratio is 23.2 and 18.5 for the ST-V and BASIII types, respectively, for 0.7 Å X-rays, and 24.0 and 19 for 1.0 Å X-rays. These results suggest that the ST-V-type imaging plates can produce 25–30% better quality of data from protein crystals than the BASIII-type imaging plates. These values are not changed much about the voltage range between 400 and 700 V against the photomultiplier. Thus, normally 500 V is supplied to the photomultiplier but, in order to obtain a large dynamic range, 400 V must be suitable. A summary of the comparison between BASIII-type and ST-V-type imaging plates is shown in Table 7.

We conclude that ST-V-type imaging plates can produce higher quality data than BASIII-type imaging plates for X-ray data collection from protein crystals using 1.0 or 0.7 Å X-rays without appreciable deterioration of the spatial resolution.

## 5. Design of an automated protein data-collection system with large-format imaging plates

The data-collection system described above can be used effectively for recording very accurate data up to the high-resolution region with high speed. However, since the system is not automatic, two or three people are required for various manual tasks during data collection. We have previously reported the design of a conveyor-belt-type automation system (Sakabe, 1991). However, it is very hard to increase the reading speed of the imaging plates; hence, it remains difficult to use synchrotron radiation with maximum efficiency. We are currently designing and developing a new type of automated (on-line) data-collection system which has high accuracy, high resolution and high speed. This fully automated system consists of a Weissenberg-type camera, an imaging-plate reader equipped with multi-reading heads which will be set at intervals of less than 10 cm, an imaging-plate eraser, and a cassette transportation

table, as shown in Figs. 4(a) and 4(b). In the new system one imaging plate is fixed onto the inside of a movable cylindrical cassette. The cylindrical cassette has 36 small rectangular holes ( $1 \times 10 \text{ mm}^2$ ) at equal intervals along the circumference of the cylinder. A primary X-ray beam passes through two holes on the cassette and shield and is diffracted by a sample crystal. Fig. 5 shows an example of how the diffraction spots are recorded on the imaging plate. The exposure area on the imaging plate can be selected by two upper and two lower screens. There are two selections of the exposure area, namely an asymmetric setting and a symmetric setting, which are shown in Figs. 5(a) and 5(b), respectively. In these figures the exposure area is  $20^\circ$  and the X-ray beam passes through hole number 1 and diffraction spots are recorded on the imaging plate as dots shown in frame 1 of Figs. 5(a) or 5(b). After the first

frame has been recorded, the cassette is rotated by  $20^\circ$ . The primary X-ray beam passes through hole number 3 and diffraction spots are recorded on the area adjacent to the last exposed area, as shown in frame 2 of Figs. 5(a) or 5(b). When we set the exposure area at  $20^\circ$  and the asymmetric setting is employed, the resolution along the equatorial is  $2.8 \text{ \AA}$ , as shown in Table 8. Since the radius of the cassette is designed to be 400 mm and the length along the cylindrical axis is 500 mm, the maximum resolution along the horizontal (cylindrical axis) is  $1.89 \text{ \AA}$ . Fig. 6 shows the relation between maximum resolution along the equator on the cassette ( $2\theta$ ) and number of reflections in arbitrary units against resolution using  $1.0 \text{ \AA}$  X-rays. Considering resolutions of 1.89 and  $2.8 \text{ \AA}$ , we obtain  $2.5 \text{ \AA}$  resolution data for protein crystal structure analysis using the above conditions as shown in Fig. 6. On the other hand,

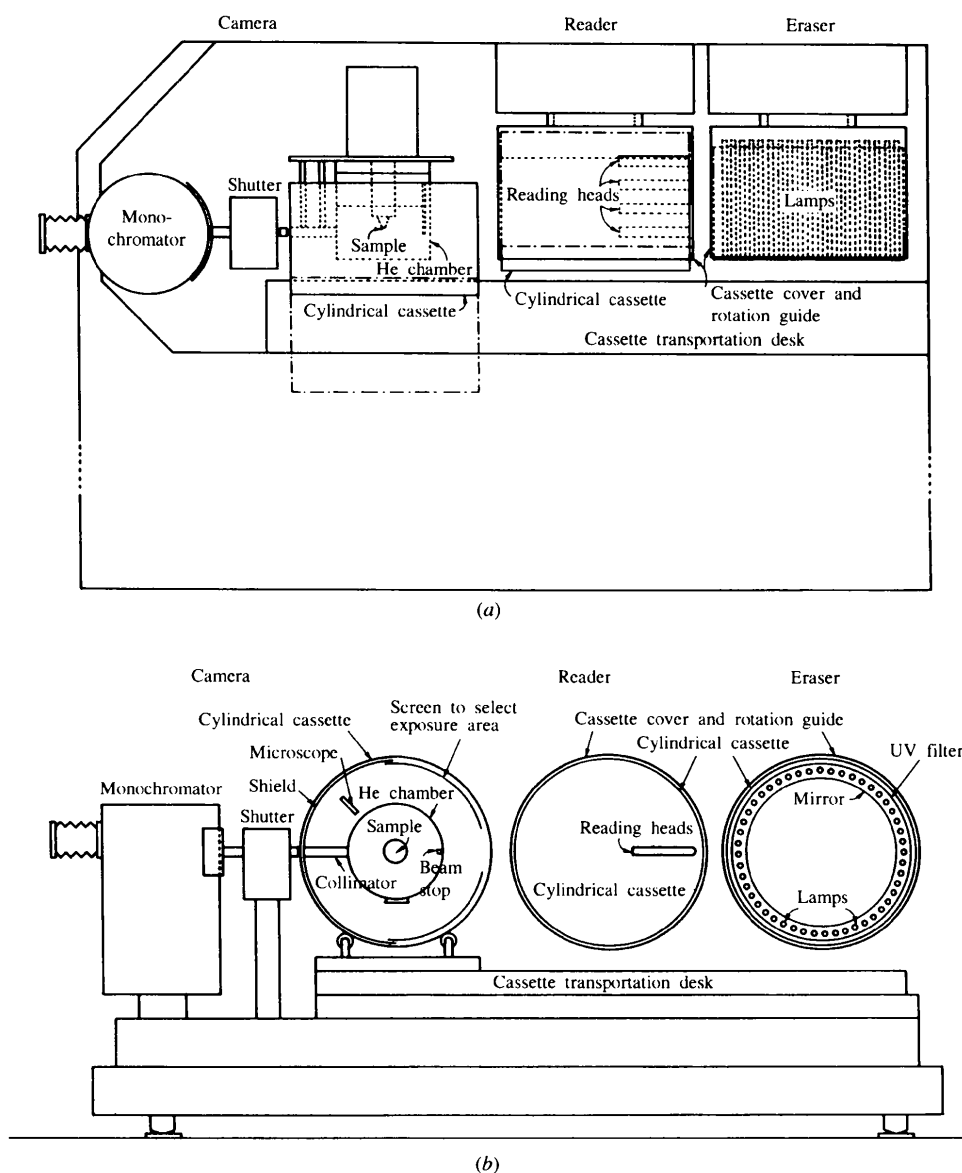


**Figure 4**  
Design concept of a fully automated protein data-collection system using an imaging plate. (a) Plan, (b) side view.

according to the user's report at the Photon Factory, data are usually collected with a  $5\text{--}10^\circ$  oscillation angle per frame. This means a full set of diffraction data of most of the protein crystals can be recorded on the imaging plate of one cassette. Assuming it takes 5 s for  $20^\circ$  rotation and setting the cassette at the measurement position, the total time for the setting per cassette (18 frames) is 90 s. When we set this data-collection system in third-generation synchrotron radiation facilities, the exposure time per frame must be less than 1 s, and we can record a full data set within 2 min in one cassette. When  $30\text{--}40^\circ$  as an area of a frame is employed, the second cassette will be necessary. In this case the time to replace the cassettes using a transfer table must be added. We estimate the time for exchanging the cassettes to be less than 4 min. Up to these conditions we can read the images after all the data have been recorded on one or two cassettes, if the speed of the reader is not so fast. However, when the angles of an area of a frame are larger than  $60^\circ$  or the cell dimensions of a sample crystal are so large that the data to be recorded exceed the capacity of

the two cassettes, the speed of the reader becomes crucial. At the present stage we are planning to achieve a cassette reading speed of less than 10 min and an image erase time of less than 6 min. Fig. 7 shows the time schedule of the continuous data collection, *i.e.* while data on one cassette are reading and erasing, another cassette is recording. Since the rate-determining step is still reading and erasing, we will speed up the steps in considering the rotation speed of the cassette, the laser power, the number of reading heads, the light source of eraser and so on.

This system therefore permits the use of synchrotron radiation X-rays with maximum efficiency, and reduces the manpower necessary for data collection with the off-line scanner.

## 6. Conclusions and discussion

We have developed a  $400 \times 800$  mm large-format imaging plate, BASIII, and its read-out system, IPR4080. The protein data-collection system with dedicated screenless

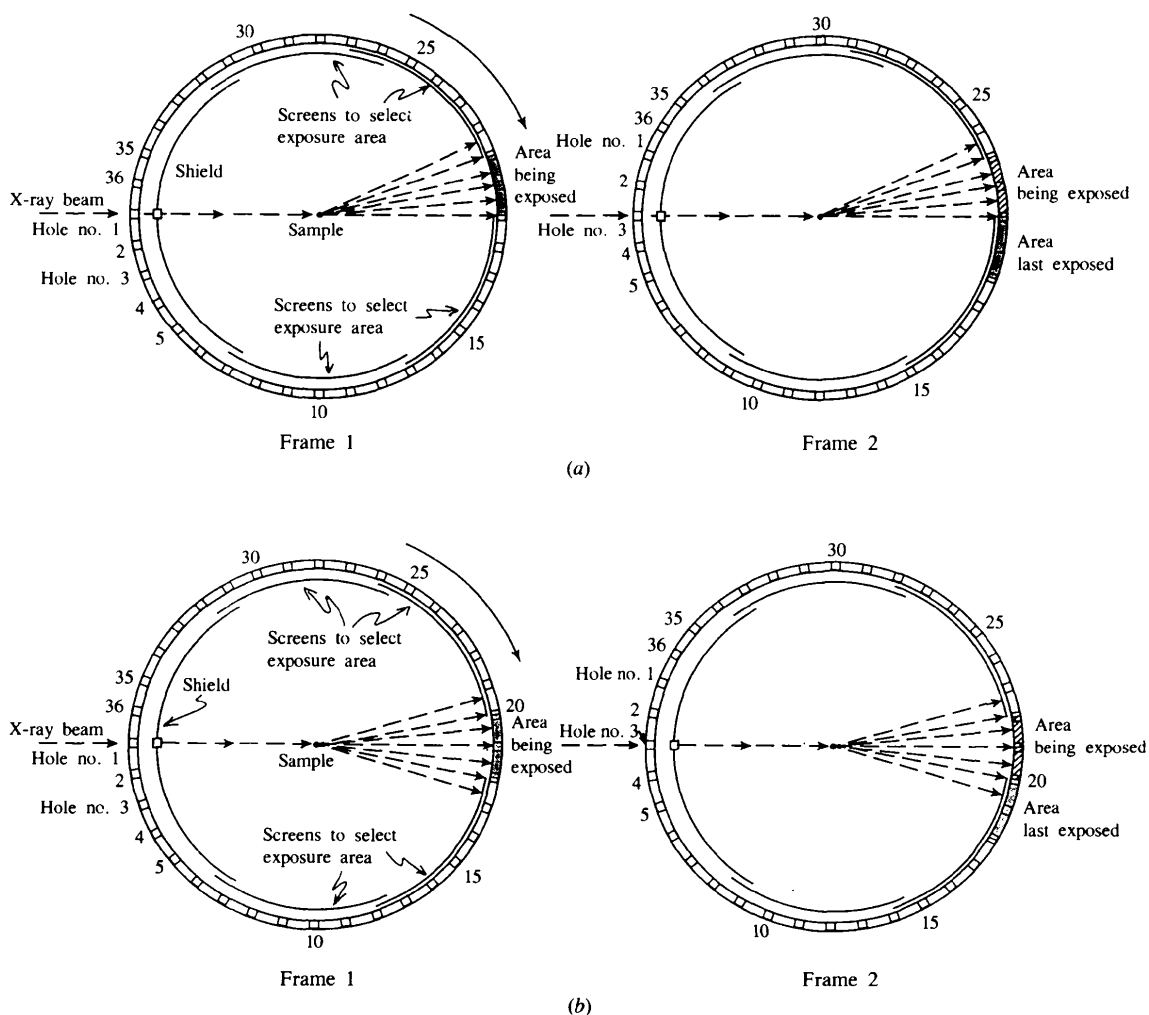


**Figure 5**

Operation of the cassette when taking  $20^\circ$  frames, viewed from the side. The small squares on the cassette represent rectangular holes for entrance of the incident X-ray beam. (a) Asymmetric setting, (b) symmetric setting.



University for preparing  $\omega$ -APT crystals, and to Dr S. Ikemizu of Tsukuba University for his assistance in the measurement of the linearity curve of IPR4080. This work was supported by a grant-in-aid for scientific research on a priority area and partly supported by JSPS under the new research support program 'Research for the Future', JSPS-RFTF96R14501.

### References

- Collaborative Computing Project, Number 4 (1994). *Acta Cryst.* D50, 760–763.
- Harada, K. (1996). Private communication.
- Higashi, T. (1989). *J. Appl. Cryst.* 22, 9–18.
- Kamiya, N., Sasaki, K., Watanabe, N., Sakabe, N. & Sakabe, K. (1997). *J. Synchrotron Rad.* 4, 14–16.
- Miyahara, J., Takahashi, K., Amemiya, Y., Kamiya, N. & Satow, Y. (1986). *Nucl. Instrum. Methods*, A246, 572–578.
- Otwinowski, Z. & Minor, W. (1996). *Methods in Enzymology*, edited by C. W. Carter Jr & R. M. Sweet, p. 276. New York: Academic Press.
- Sakabe, N. (1991). *Nucl. Instrum. Methods*, A303, 448–463.
- Sakabe, N., Ikemizu, S., Sakabe, K., Higashi, T., Nakagawa, A., Watanabe, N., Adachi, S. & Sasaki, K. (1995). *Rev. Sci. Instrum.* 66, 1276–1281.